OXFORD

SOT | Society of Toxicology
www.toxsci.oxfordjournals.org

TOXICOLOGICAL SCIENCES, 156(1), 2017, 261–274

doi: 10.1093/toxsci/kfw252
Advance Access Publication Date: January 23, 2017
Research article

Zinc oxide Nanoparticles-Induced Reactive Oxygen Species Promotes Multimodal Cyto- and Epigenetic Toxicity

Samrat Roy Choudhury,* Josue Ordaz,* Chiao-Ling Lo,† Nur P. Damayanti,* Feng Zhou,† and Joseph Irudayaraj*,[1]

*Department of Agricultural & Biological Engineering, Bindley Bioscience Center, Purdue University, West Lafayette, Indiana 47907; and †Department of Anatomy and Cell Biology, Indiana University School of Medicine, Indianapolis, Indiana 46202

[1]To whom correspondence should be addressed. Fax: (765) 496-1115. E-mail: josephi@purdue.edu.

ABSTRACT

In this study we evaluated and correlated the cytotoxic effects of zinc oxide nanoparticles (ZnO-NPs) to the epigenetic modifications, using human embryonic kidney (HEK-293) cells as a model system. Imaging of singlet and total reactive oxygen species (ROS) in ZnO-NPs-treated live cells was performed followed by the evaluation of its effects on cytoskeletal, mitochondrial, and nuclear integrity, and on the expression of ROS responsive genes. Next, we determined the global and locus-specific changes in DNA-methylation at the 3 global genomic repeat sequences namely LINE-1, subtelomeric D4Z4 and pericentromeric NBL2, and at the promoter of selected ROS responsive genes (*AOX1*, *HMOX1*, *NCF2*, *SOD3*). Our studies revealed severe actin depolymerization, increased release of mitochondrial cytochrome C, and nuclear enlargement in ZnO-NPs-treated cells. At the epigenetic level, we observed global reduction in 5-methylcytosine and increase in 5-hydroxymethylcytosine content. Additionally, we observed significant increase in the expression of Ten-Eleven Translocation (TET)-methylcytosine dioxygenase genes but not in the expression of DNA-methyltransferases (DNMTs). Based on our findings, we suggest that ZnO-NPs induce abundant increase in ROS to promote multimodal structural and functional anomalies in cells. Most importantly, ZnO-NP-induced ROS may promote global hypomethylation in cells by triggering the expression of TET-enzymes, avoiding DNMT interferences. Global DNA demethylation is considered to be the hallmark of the majority of cancers and once acquired this could be propagated to future progenies. The present study, hence, can be used as a platform for the assessment of epigenomic toxicity of ZnO-NPs in humans in the light of its use in commercial products.

Key words: ZnO-nanoparticles; cytotoxicity; epigenetics; DNA-methylation.

Engineered nanomaterials (ENMs) are defined as intentionally manufactured materials, where majority of the particles are in the size dimension of 1–100 nm (Yokel and MacPhail, 2011). The multimodal applications of ENMs are in high demand over the last few decades in textile, cosmetic, electronic, agriculture, or pharmaceutical industries (Choudhury *et al.*, 2011; Choudhury *et al.*, 2012; Gerber and Lang, 2006; Nel *et al.*, 2006). The next generation nanodevices hold further promise to bolster the industrial economy, engaged in thousands of other nano-bio interacting components (Ehmann *et al.*, 2013). However, unusual physicochemical properties, such as sub-micron size (high surface to volume ratio), supramolecular reactivity, or surface modifications of ENMs may present living systems with a uniquely novel challenge, because there have been no or limited selection pressure for immune systems to counter the adverse effects of these particles (Oberdorster *et al.*, 2004; Teeguarden *et al.*, 2007). The investigation towards exploring the mechanistic action of commonly used ENMs hence have been

unanimously commissioned among both the proponents and skeptics of nanotechnology, before their extensive usage and dissemination (Gerber and Lang, 2006; Nel *et al.*, 2006). Zinc oxide (ZnO) nanoparticles (NPs) and nanohybrids belong to one such ENMs that are frequently used in food packaging and drugs because of their superior antimicrobial efficacy (Brayner *et al.*, 2006; Jones *et al.*, 2008). ZnO nanoformulations are also being frequently used in the sun-protective lotions, wall paints, ceramic manufactures, or sporting goods (Fan and Lu, 2005; Singh and Nanda, 2014). However, a myriad of studies simultaneously reported the consequence of acute and chronic exposure of ZnO-NPs against the *in vitro* and *in vivo* cytotoxicity and genotoxicity in both plants and animals (Adamcakova-Dodd *et al.*, 2014; Lin and Xing, 2007; Wang *et al.*, 2006; Zhao *et al.*, 2009). Generation of reactive oxygen species (ROS) and induction of oxidative stress has been defined to be the major contributing factor in ZnO-NPs-mediated toxicity. Moreover, ZnO-NPs are also reported to be notoriously toxic to evoke tier-1, tier-2, and tier-3 level of oxidative stress responses, according to the hierarchical oxidative stress hypothesis (Li *et al.*, 2008; Nel *et al.*, 2006; Xia *et al.*, 2008). Assessment of ZnO-NPs toxicity, however, remained limited to the DNA damage or ROS related gene expression analysis over the past decades. In contrast, the effect of ZnO-NPs toxicity on the epigenetic modifications, which actually underlies the expression of a gene during cell growth and differentiation was not explored (Jaenisch and Bird, 2003). Epigenetic modifications, including DNA methylation, histone covalent modifications, and noncoding RNA mechanisms can often be affected by many environmental factors, including environmental contaminants, diet, stress, alcohol, radiation, and NPs toxicity (Alpatova *et al.*, 2010; Baccarelli and Bollati, 2009; Jirtle and Skinner, 2007). In particular, aberrations in DNA methylation patterns such as hyper- and hypomethylation of functional genes, which are linked to transcriptional silencing or overexpression, respectively, have been extensively studied and described as hallmarks of nearly all types of cancer and genetic disorders. It is becoming increasingly clear that even short-term exposure to environmental toxicants can alter epigenetic marks, causing heritable changes in gene expression to result in multiple abnormalities. Recent studies have reported anomalous changes in DNA methylation levels because of ENM toxicity (Baccarelli and Bollati, 2009; Perreault *et al.*, 2012). However, the mechanistic insights on alteration in aberrant DNA methylation pattern and methylation dynamics because of ENMs toxicity remain unexplored and elusive.

In the present study, we attempt to elucidate the ZnO-NPs-induced cytotoxic effects on the epigenetic aberrations namely DNA methylation in human embryonic kidney (HEK-293) cells. To achieve this aim, we evaluated the following factors in cells after 48 h of exposure with two effective cytotoxic concentrations of ZnO-NPs: (1) cell viability using MTT (3-(4,5-dimethylthiazol-2-yl)-2,5-diphenyltetrazolium bromide) based assay, (2) cell morphology and structural dynamics of cytoskeleton using microscopy and F-actin assay, (3) concentration of Zn in the culture media, (4) internalization of ZnO-NPs inside the cells, (5) induction of singlet oxygen species ($^1O_2$) and ROS, change in mitochondrial membrane potential (MMP) ($\Delta\psi M$), and nuclear enlargement using multimodal live-cell imaging and postimage-processing, (6) apoptosis with immunofluorescence, (7) expression profile of human oxidative gene cluster with qPCR, (8) genome-wide 5-methylcytosine (5-mC) and 5-hydroxymethylcytosine (5-hmC) with ELISA, (9) expression analysis of Ten-Eleven Translocation (TET) 5-methylcytosine dioxygenase and DNA-methyltransferase (DNMT) genes with qPCR, and (10) locus-specific methylation at the three genomic repeat sequences and promoters of selected oxidative stress related genes using pyrosequencing. The assembled data indicates that ZnO-NPs-induced ROS may cause severe multimodal damages to cells, and significantly introduce aberrant epigenetic alterations in treated cells.

MATERIALS AND METHODS

Preparation and Physicochemical Characterization of ZnO-NPs

ZnO-NPs were synthesized in the form of amorphous powder, followed by the guidelines of a previously published report (Wu *et al.*, 2006). Briefly, 0.5 M zinc nitrate hexahydrate [$Zn(NO_3)\cdot 6H_2O$] solution was added drop wise to equimolar sodium hydroxide solution, followed by an incubation for 2 h at room temperature (RT) under strong stirring. The resultant was centrifuged, washed alternatively with water and ethanol for three times, followed by filtration. The ZnO-NP slurry was then subjected to rotary vacuum evaporation for the removal of residual water or ethanol. The resultant product was stored in dark at RT. The distributions of hydrodynamic radius (R_H) and surface charge distribution (in terms of ζ-potential) of ZnO-NPs were analyzed after dispersing in water, using dynamic light scattering (DLS) (Zetasizer nano series: Nano-S, Malvern, Worcestershire, United Kingdom). The actual size and morphology of the synthesized particles were determined using high resolution transmission electron microscopy (HR-TEM) [FEI Technai G2, G.0] operated at 200 kV after mounting the samples on a carbon coated copper grid. The shape and size distribution of ZnO-NPs was determined using HR-TEM in 100 randomly chosen particles per observed fields.

Cell Culture and Treatment with ZnO-NPs

HEK-293 cells were seeded (0.7×10^6) in petri-plates or culture flasks in the presence of Dulbecco's modified Eagles medium (DMEM; GibcoTM) supplemented with 10% heat-inactivated fetal bovine serum (FBS), 1× glutamine (0.584 mg/l), 1× sodium pyruvate (110 mg/l), 1× nonessential amino acids, and 1% penicillin–streptomycin (Life Technologies) under 5% CO_2 at 37°C.

Cell Viability Assay

The extent of ZnO-NPs toxicity was assessed *in vitro* using MTT (3-(4, 5-dimethylthiazol-2-yl)-2, 5-diphenyl-2*H*-tetrazolium bromide) based assay using Vybrant MTT cell proliferation assay Kit (V13154; Thermo Fisher Scientific). Details of the cell viability assay can be found in the Supplementary methods.

Analysis of Cell Morphology

The surface (membrane) deformities in cells exposed to ZnO-NPs for 48 h were visualized with Field Emission Scanning Electron Microscopy (FE-SEM) [JEOL JSM-600 F; Tokyo, Japan]. Briefly, cells were grown in 24-wells bottom-glass petriplates. Cells were washed two times with phosphate buffer saline (PBS) solution followed by fixation with 2% glutaraldehyde solution. Fixed cells were then mounted, and the images were obtained at 5.0 kV vacuum under ×3000 and ×5000 magnifications.

Measurement of Zn Concentration in Culture Media and *in vitro* Uptake

The concentration of elemental Zn in the cell culture media was determined with Inductively Coupled Argon Plasma Mass Spectrometry (ICP-MS). The sample preparation was carried out following an existing standard protocol (Shen *et al.*, 2013). The sample was introduced into the plasma using an Aridus desolvating system with a T1H nebulizer (Teledyne Cetac Technologies, Ohama, Nebraska), which is used to enhance sensitivity and reduce oxide and hydride interferences. The argon sweep gas and nitrogen of the Aridus were adjusted for maximum peak height and stability using ^{7}Li, ^{115}In, and ^{238}U peaks obtained from a diluted Exaxol multi-element standard (10 ppm, Exaxol Chemical Corporation). The ^{66}Zn and ^{68}Zn coupled through ICP-MS, and the results were obtained using an ELEMEN-2 (ThermoFinnigan, Bremen, Germany) mass spectrometer in the medium resolution mode. The *in vitro* uptake and intracellular deposition of ZnO NPs were determined by thin section TEM coupled with energy dispersive X-ray spectroscopy (EDX). Briefly, HEK-293 cells, treated with ZnO NPs for 48 h were fixed in glutaraldehyde and subjected to TEM followed by an existing standard protocol (Hondow, 2014). Energy dispersive X-ray spectra were collected from the suspected NP-clusters in the cells and analyzed for the detection of elemental Zn.

MMP ($\Delta\psi$M) and Integrity

Mitochondrial membrane potential of the ZnO-NPs-treated cells (for 48 h) were determined by quantifying the change in red aggregate over green monomer ratio of JC-1 signal. Briefly, cells were washed three times with PBS, and incubated with 7.6 μM of JC-1 and Fluorobrite dye (Thermo Scientific), respectively, per manufacturer's guidelines. Fluorescence emission for JC-1 aggregates and JC-1 monomers were collected at 590 and 520 nm, respectively. In addition, we developed a novel FLIM based method to determine the mitochondrial membrane integrity. Details of FLIM and associated information on instrumentation and image analysis can be found in Supplementary methods.

Quantification of Total ROS and Singlet Oxygen ($^{1}O_2$) Species

Cells incubated for 48 h in the presence of ZnO-NPs were selected for total ROS and $^{1}O_2$ oxygen species quantification. For total ROS determination, cells were incubated with 5 μM CellROX© orange for 30 min, followed by incubation with Fluorobrite in DMEM media per manufacturer's guidelines (ThermoFisher Scientific). Fluorescence emission of ROS was captured at 445 and 565 nm, respectively. For determining $^{1}O_2$, cells were incubated with singlet oxygen sensor green (SOSG) (Thermo Scientific) for 1 h in Minimum Essential Media (MEM) media. The MEM with SOSG was then replaced with DMEM supplemented with Fluorobrite and subjected to imaging at 488 and 520 nm, respectively. Details of microscopy and image analysis can be found in Supplementary methods.

Structural Integrity of Cytoskeleton, Chromatin Condensation, and Apoptosis Assay

Cells treated with ZnO-NPs for 48 h were washed three times with PBS buffer and fixed with 4% paraformaldehyde solution. Fixed cells were then permeabilized with 1% Triton X-100 for 45 min at RT, followed by blocking with normal goat serum solution for another 45 min. Cells were then stained with 5 μg/ml mouse IgG anticytochrome C (BioLegend) for 20 h at RT followed by counterstaining with Alexa Fluor 594 Goat antimouse antibody for 90 min in the dark at RT. Selective, high affinity F-actin probe (ActinGreenTM ready probes (ThermoFisher Scientific, R37110), and Hoechst dye (1 μg/ml) were used for staining F-actin and DNA, respectively. These dyes were added together after 1 h and 10 min, respectively, toward the end of 90 min incubation of cells, with Goat antimouse antibody. After incubation, fluorescence emission from Hoechst dye, Phallodin dye, and cytochrome C were obtained at 461, 520, and 617 nm, respectively. Details of microscopy and image analysis can be found in Supplementary methods.

Gene Expression of Oxidative Stress Responsive Gene Cluster

The mRNA expression of a panel of 84 oxidative stress responsive human genes was evaluated by using RT^2 profiler PCR array (PAHS-065Z, QIAGEN; www.sabiosciences.com/rt_pcr_product/HTML/PAHS-065Y.html; last accessed December 6, 2016) from both the control and ZnO-NPs-treated cells. Briefly, the total RNA was extracted from the 48 h post-treated cells using RNeasy Mini Kit (74104, QIAGEN) and converted to the c-DNA templates using RT^2 First Strand Kit (330401, QIAGEN). The change in fold expression of gene cluster was then determined in RT^2 SYBR green master mix, using quantitative real-time PCR (qPCR) (StepOnePlus Real-Time PCR Systems; v 2.0 Applied Biosystems). Amplification conditions were 95 °C for 10 min, followed by 40 cycles at 95 °C for 15 s and 60 °C for 1 min.

Determination of Genome-Wide 5-Methylcytosine (5-mC%) and 5-Hydroxymethylcutosine (5-hmC%)

Genomic DNA content from control (nontreated) and ZnO-NPs-treated cells (48 h) was isolated by using DNeasy Blood & Tissue kit (69504; Qiagen) according to manufacturer's instruction. The concentration of eluted DNA samples was then determined by a Nano-Drop spectrometer (1000 system; Thermo Scientific). DNA integrity and RNA contamination were assessed by gel electrophoresis. Genome-wide methylation (5-mC%) and hydroxymethylation (5-hmC%) level in the isolated DNA samples were determined with MethylFash Quantification Kits (Epigentek, New York) according to manufacturer's protocol from 100 ng of DNA in triplicate. Methylated and unmethylated DNA (20 μg/ml each) sample was used as a reference for determining the relative levels (compared with control) of 5-mC or 5-hmC in each sample.

Determination of TET and DNMT Expression

The expression of *TET* (*TET1*, *TET2*, and *TET3*) and *DNMT* (*DNMT1*, *DNMT3A*, and *DNMT3B*) genes were evaluated in comparison to the endogenous control GAPDH, from the ZnO-NPs-treated cells after 48 h at concentrations of 25 and 50 μg/ml, respectively, compared with nontreated cells. Primer sequences for GAPDH, TET, and *DNMT* genes are summarized in Supplementary Table 2. Briefly, the total RNA was extracted from post-treated cells using RNeasy Mini Kit and converted to cDNA templates using Quantitect Reverse Transcript PCR (205311, QIAGEN). The change in fold expression of *TET* and *DNMT* genes were then determined in SYBR green master mix (Life Technologies), using quantitative real-time PCR (qPCR) (StepOnePlus Real-Time PCR Systems; v 2.0 Applied Biosystems). Amplification conditions were 95 °C for 1 min, followed by 40 cycles at 95 °C for 15 s and 60 °C for 1 min.

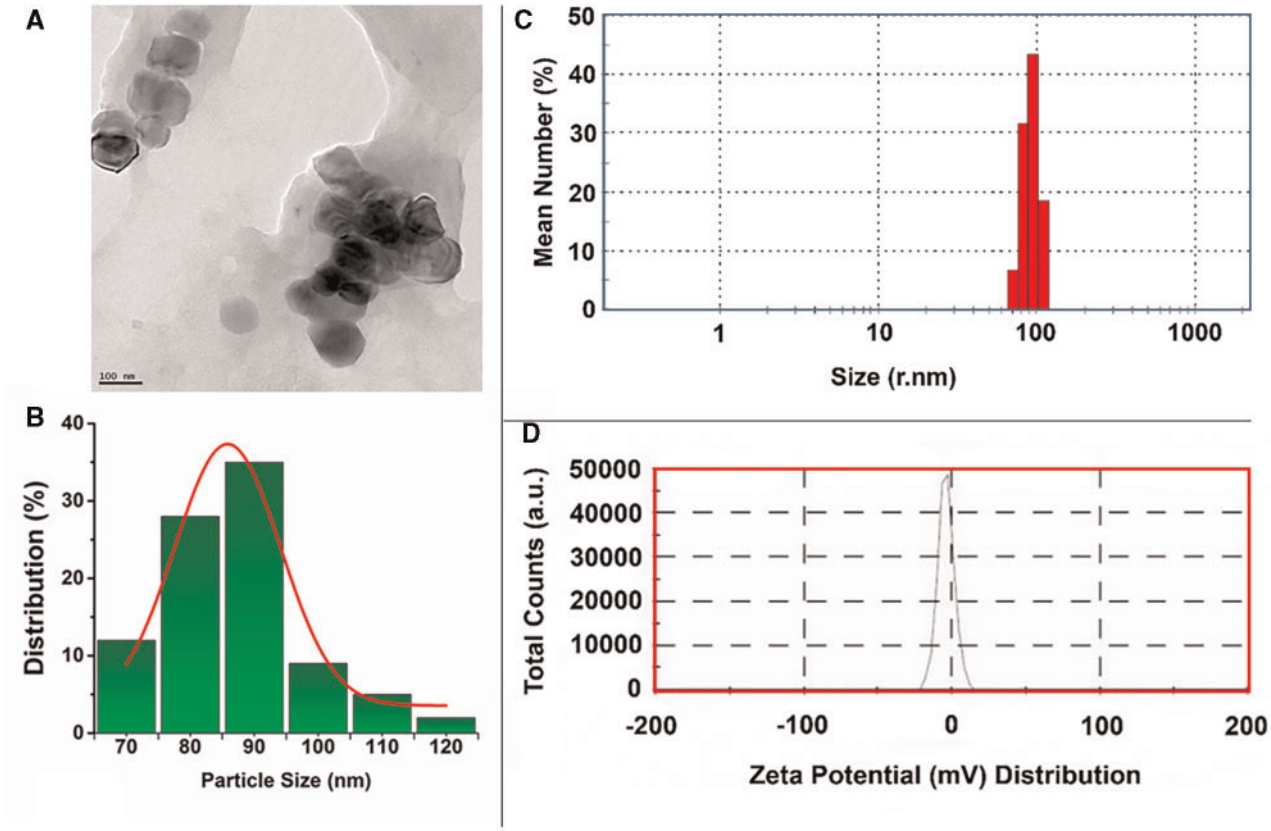

FIG. 1. Transmission electron microscopy image of ZnO-NPs (A) and their size distribution (B). The distribution of hydrodynamic radius (C), and (zeta) ζ-potential (D) of ZnO-NPs.

Each sample was assayed in triplicate from three independent round of experiments.

Bisulfite Conversion of Genomic DNA

Genomic DNA isolated from cells were bisulfite converted using the EZ DNA methylation kit (Zymo Research, California). Briefly, 500 ng of DNA sample was mixed with 5 μl of M-dilution buffer in a total volume of 50 μl and incubated at 37 °C for 15 min. A total 100 μl of Cytosine to Thymidine (CT) conversion agent was then added to the samples and incubated further at 50 °C for 14–16 h. Modified DNA was purified using Zymo spin columns along with the provided buffers. The bisulfite converted DNA samples were then eluted in 10 μl of elution buffer and evaluated for DNA concentration.

Determination of Locus-Specific Methylation Using Pyrosequencing

Bisulfite converted DNA were amplified using polymerase chain reaction (BSP-PCR) and subjected to pyrosequencing to quantitatively determine the percentage of methylation at the target CpG sites of the selected (based on their mRNA expression) ROS responsive gene promoters and three genomic repeat elements namely global LINE-1, pericentromeric NBL2 and subtelomeric D4Z4. PCR primers, reaction conditions, sequencing primers, and the analyzed sequences are summarized in Supplementary Tables 3 and 4.

Statistical Analysis

To determine the difference between average mean values between control and ZnO-NPs treated cells, a two-tailed Student's *t* test was performed. A *P*-value of $<.05$ was considered statistically significant for all the obtained data.

RESULTS

Characterization of ZnO-NPs in the Colloidal Media

TEM micrographs revealed synthesized ZnO-NPs were spheroid in shape (Figure 1A) with the average particle size in the range between 70 and 120 nm (Figure 1B). However, the size of majority of NPs was determined to be ~90 ± 2 nm. In contrast, the hydrodynamic radii (R_H) of ZnO-NPs in the Millipore water were found to be distributed in the range between 85 and 130 nm (Figure 1C). Disparity in size distribution between the two methods indicates a tendency of flocculation among particles in the colloidal media. The surface charge (ζ-potential) distribution of ZnO-NPs was in the range between ±5 mV, which suggests a rapidly aggregating nature of NPs in the colloidal media (Figure 1D).

Cell Viability Assay

For determining the effective cytotoxic dosage of the synthesized ZnO-NPs, we started from the concentration of 6.25 μg/ml with 2-fold increase in dosage up to 100 μg/ml. However, we observed no sign of cytotoxicity at doses lower than 25 μg/ml, and majority of cell death at 100 μg/ml (data not shown). MTT data represent the effect of ZnO-NPs on cell viability at

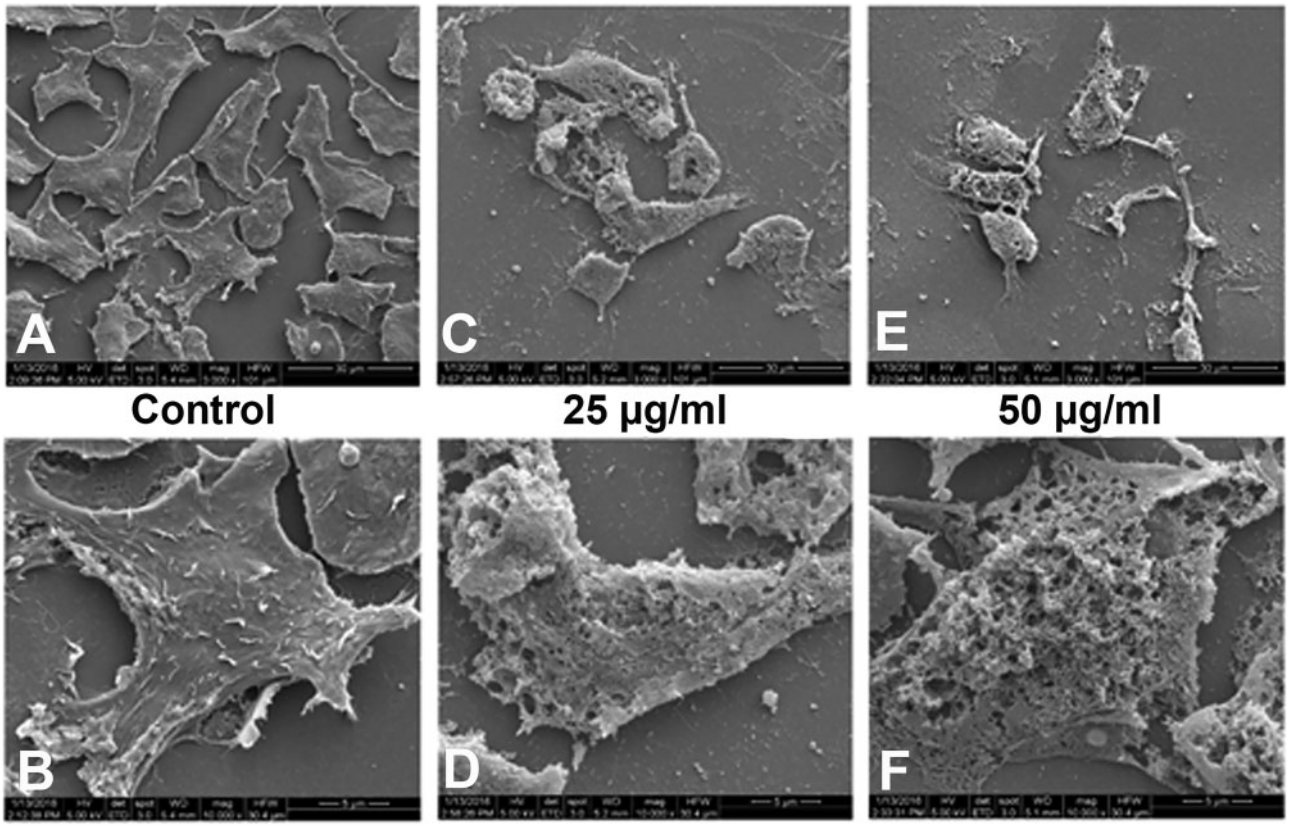

FIG. 2. Field Emission-Scanning Electron Microscopy (FE-SEM) images represent cell-surface deformities in the ZnO-NPs treated cells at a concentration of 25 µg/ml (C, D) and 50 µg/ml (E, F), respectively, compared with the nontreated (control) cells (A, B).

concentrations of 25 and 50 µg/ml (Supplementary Figure 1). Zinc oxide nanoparticles caused significant ($p < .05$) reduction in cell viability at a concentration of 25 µg/ml compared with the control after 24 h of exposure. The cells, however, seem to be more tolerant to this concentration after 48 h of incubation. In contrast, cell viability was significantly reduced at a concentration of 50 µg/ml, after 24 and 48 h of incubation with the NPs. Cell viability determined at the two aforementioned end-points also differed significantly between the cells treated with 25 and 50 µg/ml of ZnO-NPs.

ZnO-NPs Effects on Structural Dynamics of Cytoskeleton

We observed severe deformities at the surface of NP treated cells, compared with their untreated counterpart (Figure 2). FE-SEM micrographs revealed an increasing degree of porosity and roughness in the cell membrane along with the increasing concentration gradient (Figure 2D and F) of NPs. It was also evident from the micrographs that under toxic exposure of ZnO-NPs, cells lose their intercellular adhesion properties. Both the cell viability and FE-SEM micrographs cumulatively suggested that synthesized ZnO-NPs are most possibly acutely toxic to the cells and might have severe adverse effects on the structural dynamics of cytoskeleton. Effect of ZnO-NPs treatment on cytoskeletal deformities was further investigated in terms of F-actin polymerization in treated cells. We observed distinct polymerized actin filaments in untreated cells (Figure 4A), whereas cells treated with ZnO-NPs, showed depolymerized actin fibers (Figure 4B and C). We also observed the highest fraction of actin fragmentation or depolymerization in cells, treated with 50 µg/ml of ZnO-NPs.

Presence of Zn in Culture Media and Cellular Uptake

We determined a high concentration of Zn in the cell culture media by using ICP-MS analysis, for the highest applied concentration of ZnO-NPs, i.e. 50 µg/ml. For instance, the initial concentration of ZnO-NPs in concentrated nitric acid was approximately 25 µg/ml. After diluting to necessary 2% nitric acid concentration for ICP-MS analysis, the Zn-concentration was found to be 3.94 µg/ml relative to the external Zn-standard. TEM micrographs revealed severe damage and deformities at the ultrastructural level of the ZnO-NPs treated cells. In contrast to untreated cells (Figure 3A and B), disintegrated cellular membrane, and internal organelles were observed among the treated cells (Figure 3C). In addition, we observed clustered localization of ZnO-NPs, throughout the cytoplasm of treated cells (Figure 3E). The presence of ZnO-NPs in the suspected clusters was further confirmed using EDX (Figure 3D). From the EDX spectra of randomly selected clusters, we detected around 33.2 ± 2 wt% of elemental Zn. However, any specific site of deposition of the ZnO-NPs inside the cells was not possible, because of severe damages at the ultrastructural level.

Mitochondrial Membrane Integrity and Potential

An increase in fluorescence lifetime of the Mitotracker dye in treated cells was observed (Supplementary Figure 2B and C), compared with the untreated counterpart (Supplementary Figure 2A). Based on previous studies (Ramadass and Bereiter-Hahn, 2008), we hypothesize that an increase in fluorescence lifetime (Supplementary Figure 2C and D) may be inversely proportional to the MMP. To confirm this hypothesis, we performed

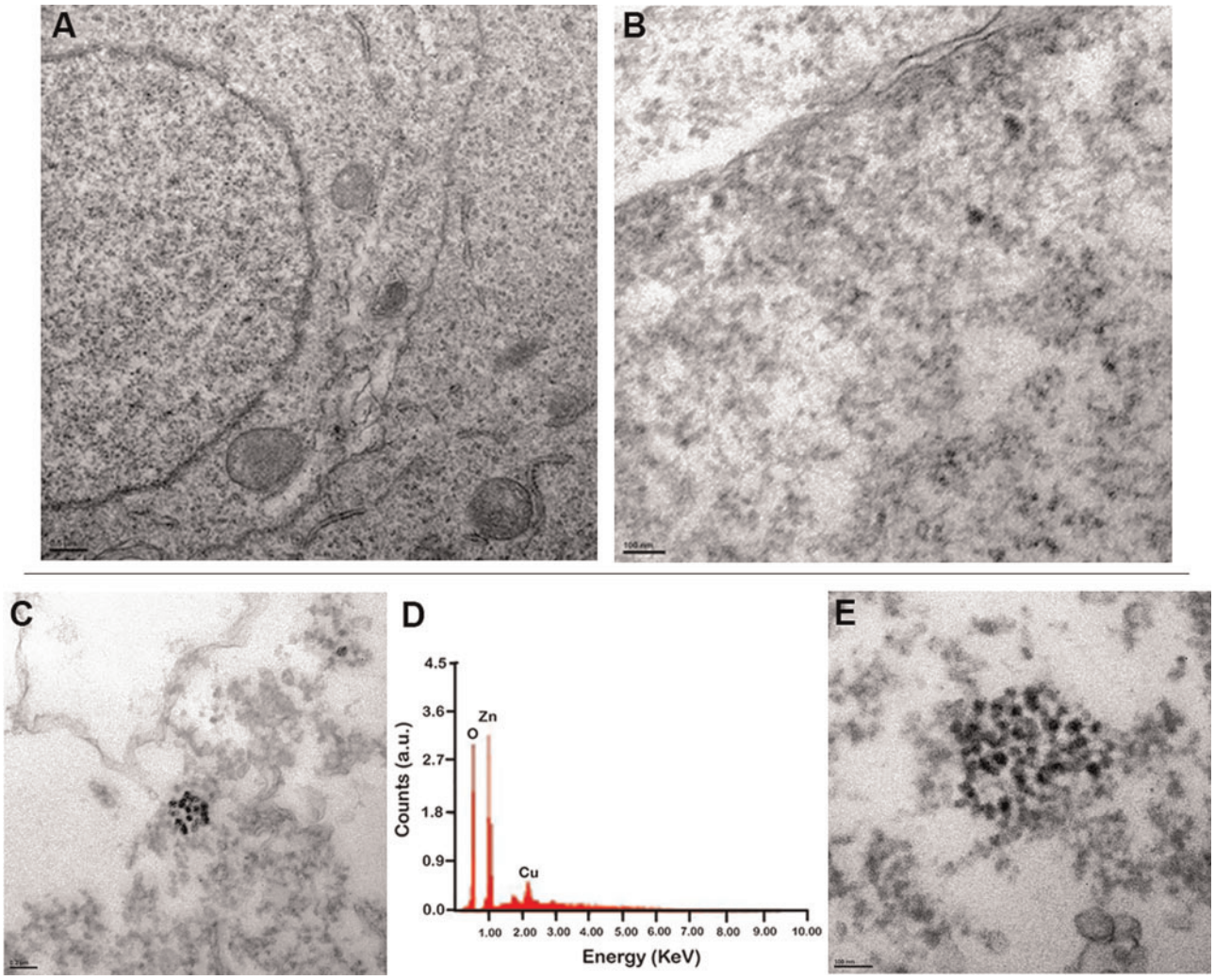

FIG. 3. Transmission electron microscopy micrographs represent the internalization of ZnO NPs inside cells (C, E), in comparison to the untreated cells (A, B). Energy dispersive X-ray spectra, coupled to TEM further confirms the presence of elemental Zn among the suspected deposition of ZnO NPs. Transmission electron microscopy scale are at 100 nm.

the established JC-1 dye-based assay using live cell imaging to corroborate the change in MMP ($\Delta\psi M$). We observed hyperpolarized mitochondrial membrane in nontreated cells, as indicated by high ratio of red intensity (J-aggregates) over green monomer intensity (J-monomers) (Supplementary Figure 2F). In contrast, a decline in J-aggregate signal accompanied by an increase in J-monomer signal was observed in treated groups (Supplementary Figure 2G and H). Quantification of the ratio of J-aggregate over J-monomer (Supplementary Figure 2I) confirmed a significant depolarization in $\Delta\psi M$ in cells, treated with 25 μg/ml ($\alpha = 0.05$; $p = 2.1E{-}218$) and 50 μg/ml ($\alpha = 0.05$; $p = 1.25E{-}20$) of NPs, compared with control. In addition, there was significant decrease ($\alpha = 0.05$; $P = .03$) in $\Delta\psi M$ between the cells treated with 50 μg/ml of ZnO-NPs, compared with the cells treated with 25 μg/ml of ZnO-NPs.

Apoptosis Assay

In a lateral expansion, we aim to determine the effect of ZnO-NPs on the release of cytochrome C from the mitochondrial membrane. We observed discrete distribution of cytochrome C signal, primarily localized in the mitochondria, in nontreated cells (Figure 4D). In contrast, a dose-dependent diffuse distribution of cytochrome C was observed among the ZnO-NPs treated cells (Figure 4E and F). The diffused distribution of cytochrome C indicates its cytoplasmic release from the mitochondria, which may lead to apoptosis.

Effect of ZnO-NPs on Nuclear Deformities

Simultaneously, we observed chromatin clumping and nuclear enlargement in the ZnO-NPs treated cells (Figure 4H and I), compared with the control cells (Figure 4G), when stained with the Hoechst DNA staining dye. This study indicates that ZnO-NPs may contribute to an increase in DNA content.

Intracellular Generation of ROS and $^1O_2$ Species

In nontreated cells, both ROS and $^1O_2$ sensor signals were observed in the mitochondria. Interestingly, in treated cells, we observed a slight diffusion of both ROS and $^1O_2$ from mitochondria to cytoplasmic compartment. Simultaneously, a dose dependent increase of both ROS and $^1O_2$ indicator intensity were also observed in treated cells (Figure 5E and H). From the whole-image intensity mapping, we quantified an increase in the

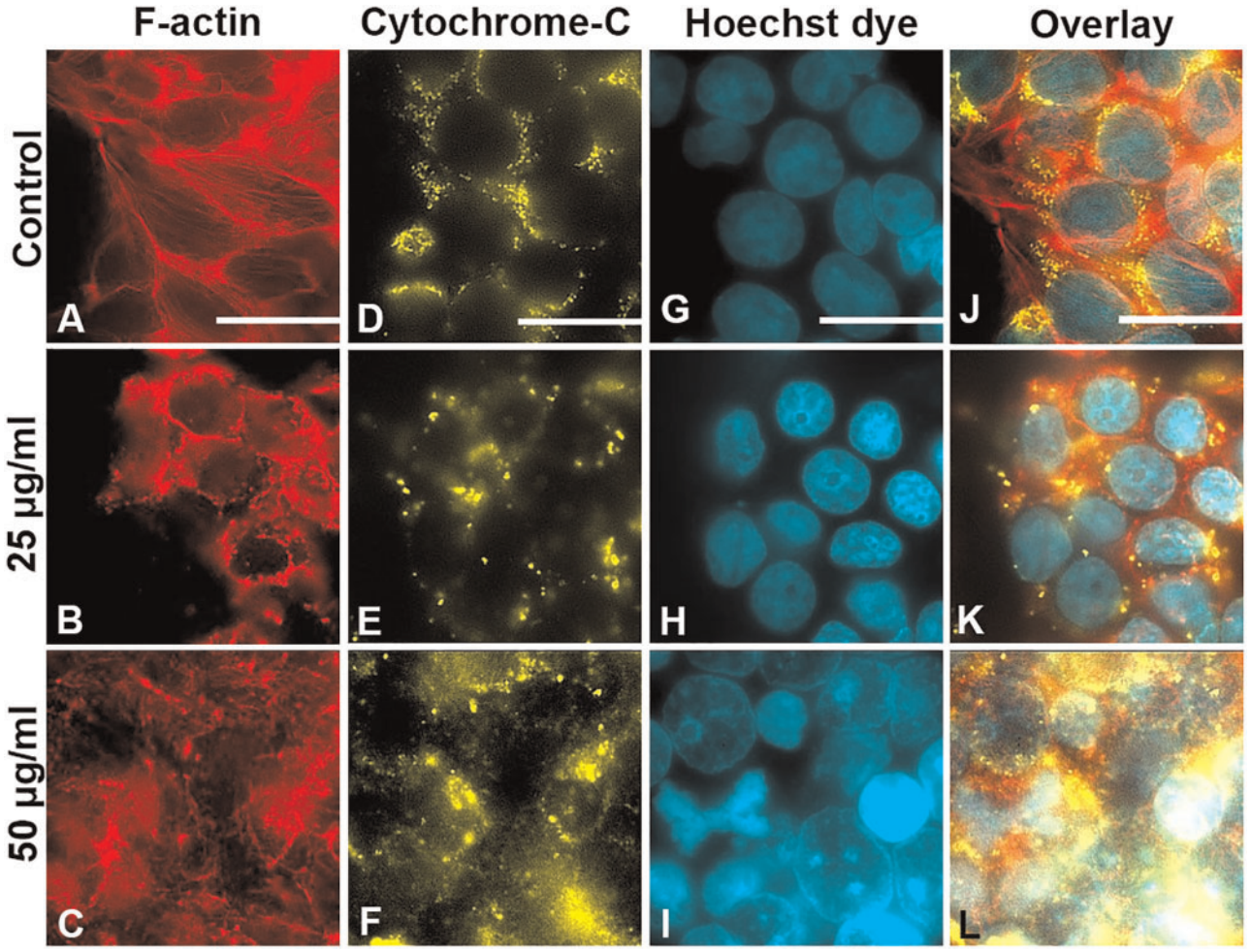

FIG. 4. Structural dynamics of cytoskeleton (in terms of F-actin polymerization) was determined in ZnO-NPs treated cells at a concentration of 25 μg/ml (B) and 50 μg/ml (C), respectively, compared with nontreated (control) cells (A). Release of cytochrome C from the mitochondrial membrane in ZnO-NPs treated (E, F) and control (D) cells. Enlargement of nucleus and chromatin compaction was observed in the ZnO-NPs treated cells (H, I), compared with control cells (G). Overlay of F-actin, cytochrome C, and nuclear structure from the control (J) and treated cells (K, L).

signal of ROS at 25 μg/ml ($\alpha = 0.05$; $p = 1.3E{-}4$) (Figure 5F) and 50 μg/ml ($\alpha = 0.05$; $p = 2E{-}6$) (Figure 5I) of the ZnO-NPs treated cells, compared with the control (Figure 5C). Likewise, an increase in the SOSG was observed at 25 μg/ml ($\alpha = 0.05$; $p = 1.6E{-}4$) (Figure 5N) and 50 μg/ml ($\alpha = 0.05$; $p = 1.7E{-}6$) (Figure 5P) of the ZnO-NPs treated cells, compared with control (Figure 5I).

Expression Profile of Oxidative Stress-Related Genes

We determined the expression of 84 oxidative stress responsive genes in ZnO-NPs treated HEK-293 cells for 48 h. We observed up-regulated expression of several genes (Supplementary Table 1). For convenience, 4 out of the 84 genes, which were significantly up regulated (>4-fold; $P < .05$) with ZnO-NPs treatment (Table 1) were selected for epigenetic studies.

For instance, aldehyde oxidase 1 (*AOX1*), which increased in expression over 6-fold is a well-known xenobiotic metabolizing protein that produces excess ROS. *AOX1* also promotes cell damage, apoptosis, and fibrogenesis (Neumeier *et al.*, 2006). In contrast, Heme oxygenase-1 (*HMOX*-1), superoxide dismutase 3 (*SOD3*), and neutrophil cytosolic factor-2 (*NCF2*), which are responsible for antioxidative, and anti-inflammatory properties, were also significantly increased (Gornicka *et al.*, 2011; Sarkar *et al.*, 2007; Sharma *et al.*, 2009).

Epigenetic Toxicity of ZnO-NPs: Genome-Wide Reduction in DNA Methylation

For better understanding of the impact of ZnO-NPs-induced ROS on the genome-wide methylation, we started with the quantification of genome-wide 5-mC content in treated cells. We observed significant dose-dependent reduction in 5-mC in treated cells, compared with the nontreated ones (Figure 6A). The percentage of 5-mC level in cells treated with 25 and 50 μg/ml of ZnO-NPs, reduced by 0.9% and 1.2%, respectively, compared with the nontreated cells ($P < .05$). Next, we determined the change in global 5-hmC level in treated cells (Figure 6A). Results show that the 5hmC level increased significantly ($P < .05$) in cells, treated with ZnO-NPs at a concentration of 50 μg/ml, compared with control cells. However, we did not observe any remarkable increase in the 5-hmC level in the cells, treated with 25 μg/ml of ZnO NPs, compared with the control.

To evaluate the possible involvement of *TET* and *DNMT* enzymes in the observed methylation changes, the expression of three *TET* and *DNMT* genes were evaluated in treated cells. We

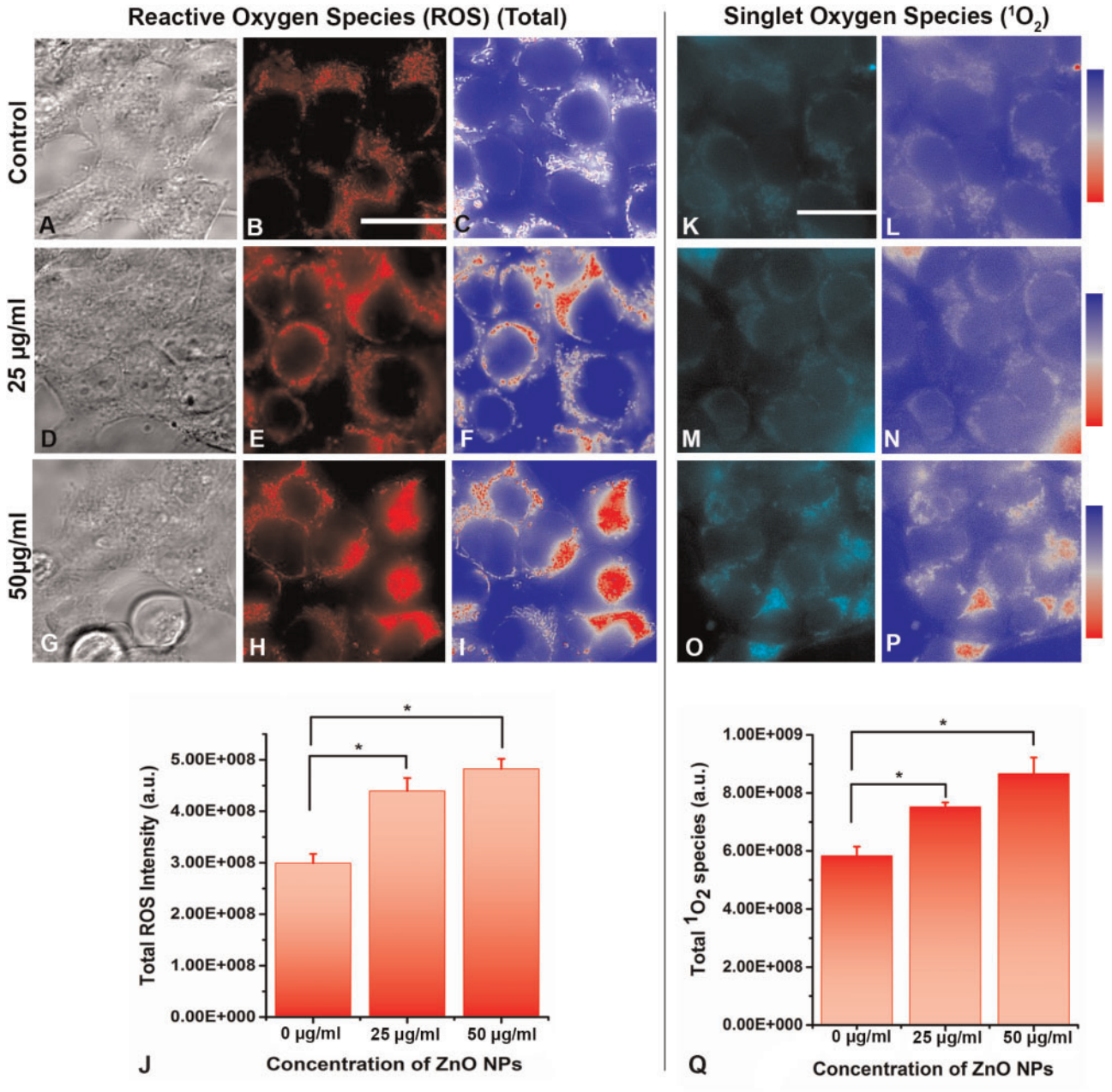

FIG. 5. Determination of total ROS and singlet oxygen ($^1O_2$) species from the control (A, B, K) and ZnO-NPs treated cells at a concentration of 25 µg/ml (D, E, M), and 50 µg/ml (G, H, O), respectively. Image mapping analysis was performed in both control (C, L) and treated cells (F, I, N, P) to quantify the changes in total ROS (J) and $^1O_2$ (Q) in cells.

TABLE 1. The Significant Up Regulation (over 4-fold) in Transcript Expression of Oxidative Stress Responsive Genes, as Obtained from RT^2 Profiler PCR Array

Gene	Description	Fold Change	P-value (<.05)
AOX1	Aldehyde oxidase 1	6.86	.004
HMOX1	Heme oxygenase 1	12.36	.047
NCF2	Neutrophil cytosolic factor 2	4.53	.021
SOD3	Superoxide dismutase 3	6.05	.031

observed over 3.5-fold increase in *TET1* and around 2.5-fold increase in *TET2* expression (Figure 6D). Upregulation of both *TET1* and *TET2* genes were significant in cells ($P < .05$), treated with 50 µg/ml of ZnO-NPs, compared with nontreated cells. However, we did not observe the expression in *TET3* genes. *TET3* was not detected most possibly because of their trace amount or nonfunctionality in embryonic cells (Huang *et al.*, 2014). Additionally, we evaluated the expression of all of the candidates of *DNMT* family and observed a slight reduction in the expression of all of the *DNMT* genes (Figure 6C).

Locus-Specific Methylation Analyses

We determined changes in methylation level at locus-specific resolution with pyrosequencing analysis of the bisulfite converted genomic DNA. We quantified the methylation level of

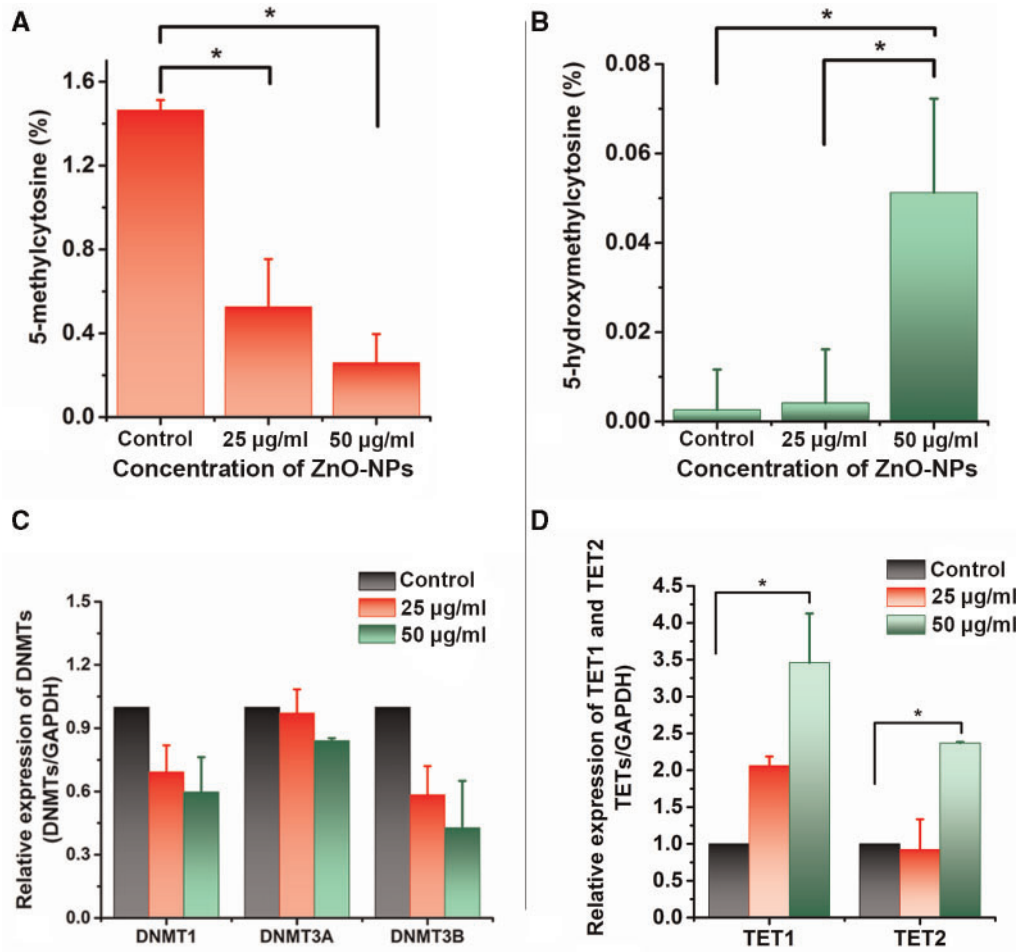

FIG. 6. Quantification of 5-methylcytosine (A) and 5-hydroxymethylcytosine in control and ZnO-NPs treated cells (B). The expression of DNMT (C) and TET (D) genes in the control and ZnO-NPs treated cells.

the 3 genomic repeat sequences namely global LINE-1, pericentromeric NBL2, and subtelomeric D4Z4 (Chr. 4q35). LINE-1 methylation, which constitutes about 40%–50% of the entire genome showed significant reduction ($P < .05$) in methylation at CpG-2, CpG-3, and CpG-4 (Figure 7A) in ZnO-NPs treated cells, at a concentration of 50 µg/ml. For instance, the methylation levels in treated cells were reduced by 9% at CpG-2 and CpG-3, and 8% at CpG-4. For the D4Z4, to a lesser extent yet significant demethylation was observed at CpG-2 (Figure 7B). For NBL2, we observed reduction in methylation by 8% at CpG-2 and 22% at CpG-5 in treated cells (Figure 7C).

We also evaluated possible changes in promoter methylation of the 4 oxidative stress related genes namely *AOX1*, *HMOX1*, *NCF2*, and *SOD3*. The sequenced promoter regions of these genes were variously distant from their respective transcription start sites (Figure 7D–G). However, we did not observe any significant changes in the promoter methylation of these genes.

DISCUSSION

Till date, the majority of the studies on ZnO-NPs is limited to cytotoxic and genotoxic properties of NPs. It is also reported that the uptake and deposition of ZnO-NPs in animals occur mainly in kidney, which may potentially interfere with blood urea nitrogen and creatinine levels and disrupt the detoxification machinery of the body (Pujalté *et al.*, 2011; Wang *et al.*, 2009). However, beyond the level of cytotoxicity and genotoxicity, less empirical information is available on the causal relationship between ZnO-induced epigenetic toxicity and eventual downstream effects at the genetic or cellular level. Herein, we present a comprehensive report on the toxic effects of ZnO-NPs at 3 different tiers namely cellular, genetic, and epigenetic (Figure 8). Cumulative data suggest a tight correlation between the epigenetic changes to the cytological and genetic anomalies in ZnO-NPs-treated cells.

The synthesized ZnO-NPs, used herein showed heterogeneity (Polydispersity index >1.0) in their colloidal size-distribution, evaluated by DLS measurements in the cell culture media (data not shown). This is probably because of the incipient protein aggregation with the ZnO-NPs. The heterogeneity in size distribution could be deleterious to cells, as different size NPs can potentially bind to a broader range of biomolecules and introduce multimodal damages (Clift *et al.*, 2008; Rana and Kalaichelvan, 2013). However, below 25 µg/ml we did not notice any significant changes at the level of cell viability or epigenetic alterations (data not shown). We observed severe damages at the cell-surface including increased porosity and roughness of the cell-membrane, and significant depolymerization of the cytoskeletal F-actin (Figs. 2 and 4A–C) at the highest applied

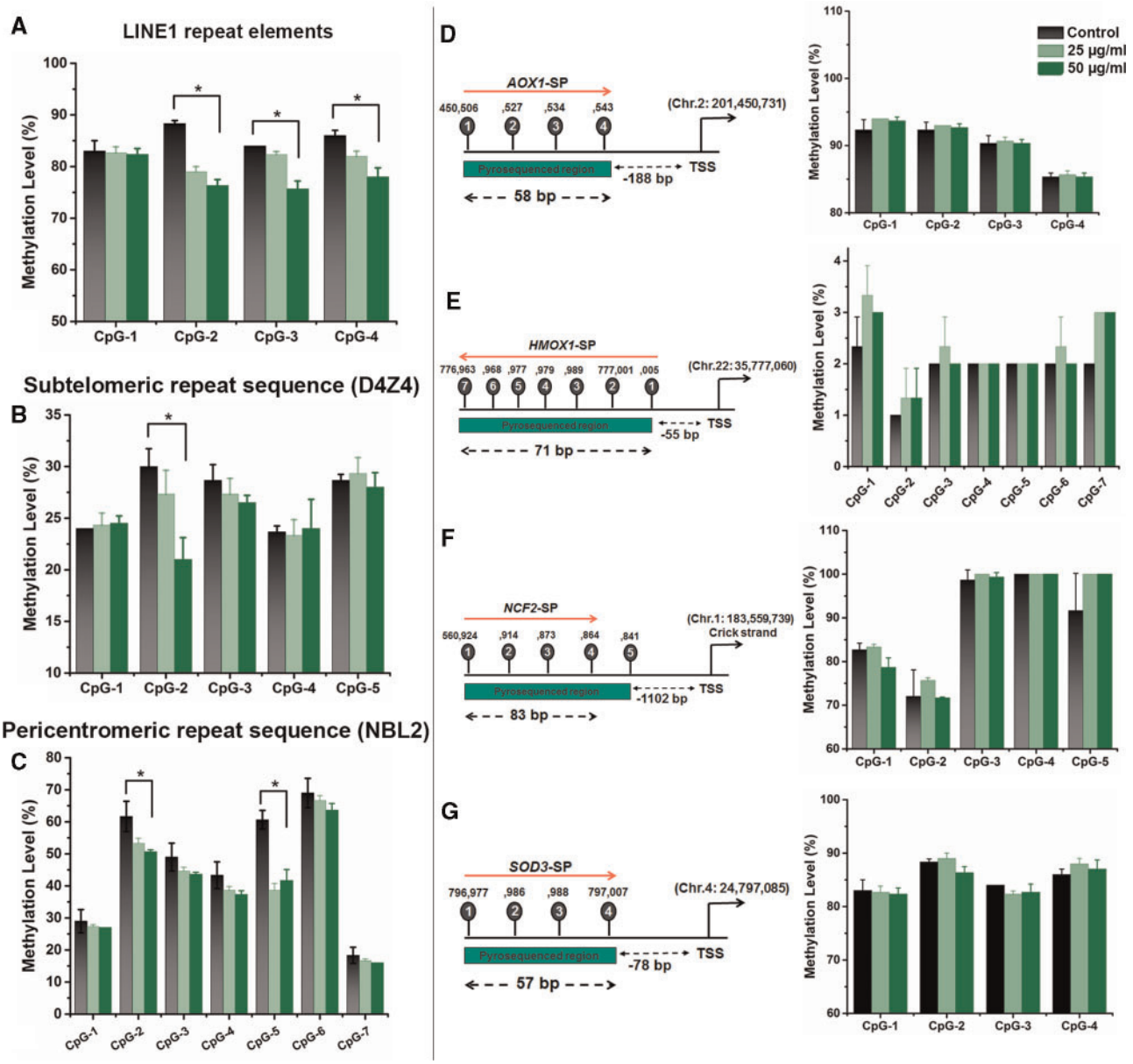

FIG. 7. Locus specific methylation level at the CpG sites in LINE-1 (A), D4Z4 (B), and NBL2 (C) repeat sequences. Level of methylation at the promoter of *AOX1* (D), *HMOX1* (E), *NCF2* (F), and *SOD3* (G) genes.

concentration, i.e. 50 μg/ml. In a lateral expansion, we also observed the internalization and *in vitro* cellular uptake of ZnO-NPs, using thin section TEM. As observed from the TEM micrographs, ZnO-NPs were distributed throughout the cytosol and caused severe deformities at the ultrastructural level in the cell.

Previous studies indicated that the loss of actin regulation dynamics plays a crucial role in the organization of cytoskeleton (Stricker *et al.*, 2010). These results indicate that ZnO-NPs may cause potential morphological and cytoskeletal damages. An impaired cytoskeletal network is shown to interrupt the interaction between actin and mitochondria (Kato *et al.*, 2010). The interaction between cytoskeletal network and mitochondria is considered to be an essential interface for mitochondrial functionalities and bioenergetics of cell (Boldogh and Pon, 2006). This led us to investigate the change in mitochondrial integrity and membrane potential (Supplementary Figure 2). To this end, we observed significant loss in the mitochondrial membrane integrity, increase in MMP, and cytoplasmic release of cytochrome C (Supplementary Figure 2; Figure 4D–F). Under multifactorial stresses, mitochondria release cytochrome C, which leads to the activation of caspases that enter the mitochondrial matrix to cleave key substrates in the electron transport chain. This ultimately leads to enhanced production of ROS (Ricci *et al.*, 2003). Our data shows that ZnO-NPs cause mitochondrial dysfunction and might promote cell death. A plethora of previous studies have also reported nuclear enlargement as an obvious sign of genotoxicity. For instance, carcinogens or chemical toxicants that induce potential breakage in DNA strands, formation of DNA adducts or frequent mutations, may eventually lead to polyploidy and nuclear enlargement (Rihn *et al.*, 2000; Westmoreland *et al.*, 1994). Zinc oxide nanoparticles are well known for their genotoxic effects (Heim *et al.*, 2015) and have

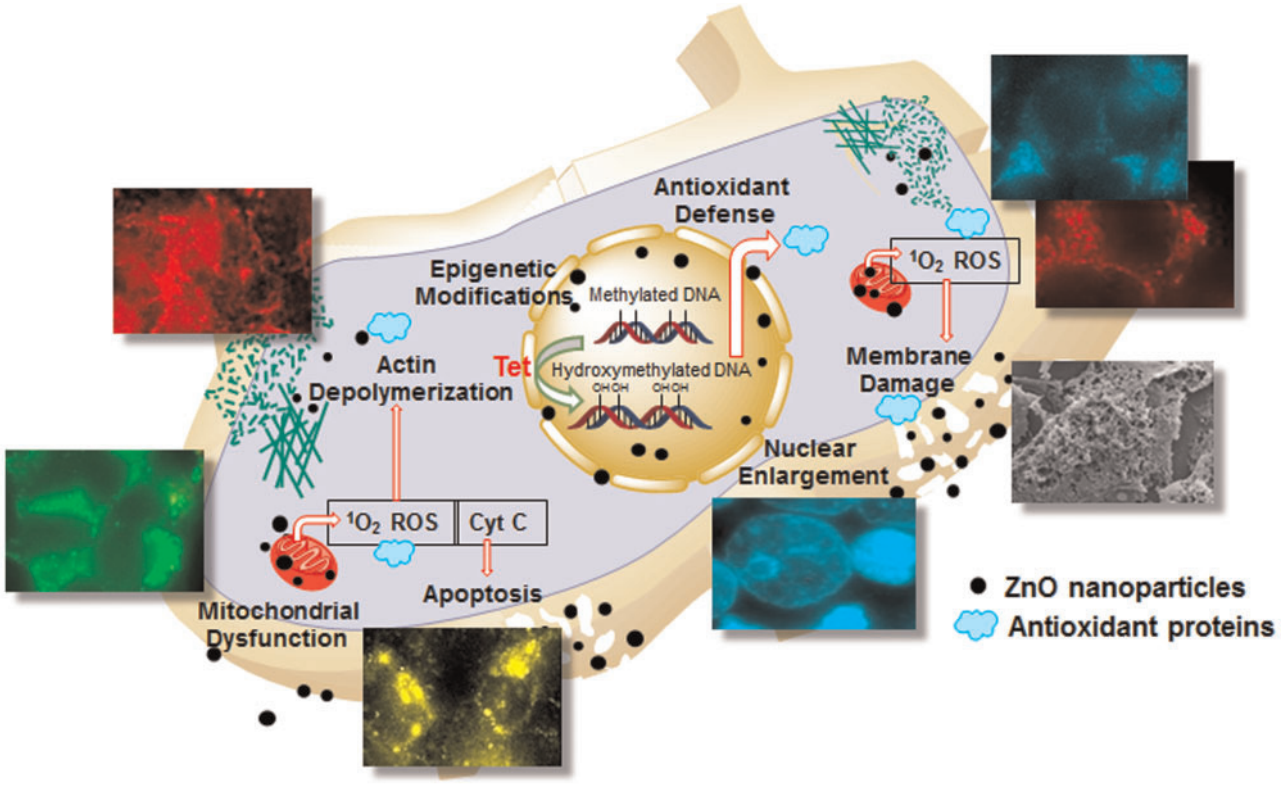

FIG. 8. A graphical illustration, representing the multimodal cyto- and epigenetic toxicity caused by the treatment with ZnO-NPs in HEK-293 cells. Zinc oxide nanoparticles induce the generation of abundant ROS including singlet oxygen species ($^1O_2$) in cells. Elevated ROS level evokes antioxidant cellular response and mitochondrial dysfunctions. The defunct mitochondria induces the leakage of cytochrome C, promote apoptosis, and other cross-talk anomalies such as actin depolymerization,. Simultaneously, we observed a trend toward the nuclear enlargement and global increase in DNA-hydroxymethylation (5-hmC) at the genetic and epigenetic level, respectively. The increment in genome-wide 5-hmC is best possibly correlated to the increase in TET enzyme activity but seemed independent of DNMT interferences.

also been reported for its potential to induce DNA fragmentation and nuclear condensation (Wang *et al.*, 2014; Wilhelmi *et al.*, 2013). The nuclear clumping and enlargement followed by ZnO NPs treatment (Figure 4G–H), as observed in the present study hence may be considered as a consequence of ZnO-NPs-induced genotoxicity.

Generation of intracellular ROS is considered as the key inducer of mitochondrial damage and oxidative stress (Nel *et al.*, 2006; Turrens, 2003; Xia *et al.*, 2008; Yu *et al.*, 2013). Simultaneously, we observed gradual increase in intracellular ROS species along with an increasing concentration gradient of ZnO-NPs (Figure 5). Based on our findings, we propose that ZnO-NPs induce intracellular $^1O_2$, which eventually aid ROS variants to elicit overwhelming oxidative stress in the treated cells. Existing studies have well-established the fact that ZnO-NPs produce abundant Zn-ions in solutions including in the cell culture. The release of Zn-ions is considered to be one of the potential inducers of ROS generation (Kao *et al.*, 2012; Shen et al., 2013; Xia *et al.*, 2008). The different species of ROS produced herein hence may also be considered as a consequence of the release of Zn-ions in the culture media. In addition, we also determined the expression of gene cluster, involved in ROS metabolism and antioxidant defense in HEK 293 cells, toxically exposed to ZnO-NPs. We observed significant upregulation of genes such as *AOX1*, compared with *HMOX1, NCF2, or SOD3*, which are antagonistic in function in terms of ROS stress management (Table 1). The coactivation of these gene are atypical for the mitochondrial stress management and can be attributed to the impaired ROS detoxifying pathways in cells, possibly because of ZnO-NPs mediated toxicity (Huang *et al.*, 2010; Sharma *et al.*, 2012). In summary, ZnO-NPs cause multimodal cytotoxic and genotoxic damages to the cells by employing the abundant generation of ROS.

Finally, we extended our study beyond the cyto- and genotoxicity level and determined the effect of ZnO-NPs on epigenetic modifications in the treated cells. Epigenetic changes are considered to be stable and heritable changes in genome. Epigenetic modifications, once imprinted in the genome may result in continued aberrant expression of a gene, being propagated to the future progenies. In particular, aberrant DNA methylation is a crucial epigenetic determinant of gene expression and function (Jaenisch and Bird, 2003). In normal cells, DNA methylation marks at the promoter of functional genes as well as heterochromatic regions are stably maintained by *DNMT1*, whereas *DNMT3A* and *3B* are engaged in *de novo* methylation (Robertson *et al.*, 1999). Herein, we determined the cytotoxic effects of ZnO-NPs on epigenomic modifications, especially in the context of DNA methylation in treated cells.

Recent studies reported that chemical toxicants may disproportionately generate ROS in cells that lead to the global decrease but selected increase in DNA methylation (Wu and Ni, 2015) at gene promoters. Both of these anomalous changes at the level of DNA methylation are considered to be a favorable microenvironment for a majority of cancer. Elevated expression of ROS could also lead to tumor development and progression of cancer involving both the genetic and epigenetic route (Campos *et al.*, 2007; Lim *et al.*, 2008; Quan *et al.*, 2011; Ziech *et al.*, 2011).

We observed significant reduction in global 5-mC (Figure 6A) and increase in 5-hmC (Figure 6B) in ZnO-NPs treated cells. Active DNA demethylation in the genome either occurs through physical removal of methyl groups from the cytosines or activity of TET family of enzymes. TET enzymes catalytically converts 5-mC to 5-hmC in the presence of 2-oxoglutarate and iron (II) excluding the *DNMT* actions (Guo *et al.*, 2011; Tahiliani *et al.*, 2009; Wu and Zhang, 2011). Significant increase in the expression of *TET* genes in the treated cells strengthens our hypothesis that ZnO-NPs may promote DNA-demethylation by involving the TET family of enzymes (Figure 6D). Moreover, we did not observe any significant changes in the expression of any of the *DNMT* genes (Figure 6C). This suggests that ZnO-NPs-induced ROS might increase TET activity excluding the *DNMT* interferences in cells.

Methylation at specific loci in the three repeat sequence elements, which are part of heterochromatin and typically harbor high level of methylation was evaluated. Reductions in methylation at these sites are in agreement with the global reduction in 5-mC content (Figure 7A–C). This also strengthens the possibility of proactive TET activity that cause genome-wide hypomethylation by inducing hydroxymethylation marks in ZnO-NPs-treated cells. In contrast, we did not observe any significant changes in the promoter methylation of the 4 oxidative stress responsive genes, which were significantly upregulated because of ZnO-NPs treatment (Figure 7D–G). The insignificant alterations in methylation at these gene promoters, however, could not be explained only with the DNMT or TET activities in cell. A few possibilities could be associated with this phenomenon. First, the generation of abundant intracellular ROS may induce activation of several TFs, which are required for antioxidative defense (Turpaev, 2002) in cells, and are independent of epigenetic regulation. In particular, Activator Protein-1 (AP-1), a generic ROS-induced TF, may be activated because of ZnO NPs treatment to regulate the expression of stress–responsive genes (Brown *et al.*, 2004). Several previous reports are available, and demonstrates the activation of AP-1 as an inducer of overexpression of genes such as *SOD*, *NCF-2*, or *HMOX-1* in ROS-stressed cells (Gauss *et al.*, 2005; Pronk *et al.*, 2014; Wenk *et al.*, 1999). This AP-1 mediated regulation of gene expression is independent of gene-promoter methylation and is a common route of cellular defense. Second, the demethylation effect of *TET* action from ZnO NPs treatment may be active at the regulatory regions, other than the promoter of a gene, such as enhancer. Finally, prolonged chronic exposure to ZnO-NPs might have caused more prominent demethylation changes at the gene promoters.

CONCLUSIONS

In this study, we investigated the effects of ZnO-NPs toxicity at the epigenetic level particularly in conjunction of DNA methylation. We observed that ZnO-NPs introduce multimodal damages to cells, including severe rupture in the cell membrane, disturbed structural dynamics of cytoskeleton, and different tiers of mitochondrial dysfunctions. Increasing concentration gradient of ZnO-NPs induce disproportionate increase of the ROS and $^1O_2$ species, which results in impairment of cellular oxidative stress management machinery. Most importantly, the generated ROS species may aid in the increase in TET activities, which result in a global reduction in DNA methylation excluding the *DNMTs* action. Correlation between ROS generation and increase in *TET* expression have been reported earlier in conjunction with other bioactive drugs and chemicals (Coulter *et al.*, 2013; Cui *et al.*, 2016; Delatte *et al.*, 2015; Zhao *et al.*, 2014). Our findings are in agreement of these previous reports. These findings clearly support that the acquired global hypomethylation because of ZnO-NPs treatment may increase the risk of a majority of cancers (Ehrlich, 2009). These epigenetic modifications, once imprinted in genome during cellular reprogramming could also potentially be inherited. This study hence demands thorough screening of ZnO-NPs against humans, before their large-scale use as an ingredient in consumables.

SUPPLEMENTARY DATA

Supplementary data are available at *Toxicological Sciences* online.

ACKNOWLEDGMENTS

This work was supported by the W.M. Keck Foundation grant and the Toxicology Pillars seed support from Purdue's EVPRP Office. Partial support from the U.S. Department of Agriculture, Agricultural Research Service, under Agreement No. 1935-42000-049-00D with the Center for Food Safety Engineering at Purdue University is appreciated.

REFERENCES

Adamcakova-Dodd, A., Stebounova, L. V., Kim, J. S., Vorrink, S. U., Ault, A. P., O'Shaughnessy, P. T., Grassian, V. H., and Thorne, P. S. (2014). Toxicity assessment of zinc oxide nanoparticles using sub-acute and sub-chronic murine inhalation models. *Part Fibre Toxicol.* **11**, 15. 10.1186/1743-8977-11-15.

Alpatova, A. L., Shan, W., Babica, P., Upham, B. L., Rogensues, A. R., Masten, S. J., Drown, E., Mohanty, A. K., Alocilja, E. C., and Tarabara, V. V. (2010). Single-walled carbon nanotubes dispersed in aqueous media via non-covalent functionalization: Effect of dispersant on the stability, cytotoxicity, and epigenetic toxicity of nanotube suspensions. *Water Res.* **44**, 505–520. 10.1016/j.watres.2009.09.042.

Baccarelli, A., and Bollati, V. (2009). Epigenetics and environmental chemicals. *Curr. Opin. Pediatr.* **21**, 243–251.

Boldogh, I. R., and Pon, L. A. (2006). Interactions of mitochondria with the actin cytoskeleton. *Biochim. Biophys. Acta* **1763**, 450–462.

Brayner, R., Ferrari-Iliou, R., Brivois, N., Djediat, S., Benedetti, M. F., and Fievet, F. (2006). Toxicological impact studies based on Escherichia coli bacteria in ultrafine ZnO nanoparticles colloidal medium. *Nano Lett.* **6**, 866–870.

Brown, D. M., Donaldson, K., Borm, P. J., Schins, R. P., Dehnhardt, M., Gilmour, P., Jimenez, L. A., and Stone, V. (2004). Calcium and ROS-mediated activation of transcription factors and TNF-a cytokine gene expression in macrophages exposed to ultrafine particles. *Am. J. Physiol. Lung Cell Mol. Physiol.* **286**, doi:10.1152/ajplung.00139.2003.

Campos, A. C. E., Molognoni, F., Melo, F. H. M., Galdieri, L. C., Carneiro, C. R. W., D'Almeida, V., Correa, M., and Jasiulionis, M. G. (2007). Oxidative stress modulates DNA methylation during melanocyte anchorage blockade associated with malignant transformation. *Neoplasia* **9**, 1111–1121.

Choudhury, S. R., Ghosh, M., Mandal, A., Chakravorty, D., Pal, M., Pradhan, S., and Goswami, A. (2011). Surface-modified sulfur nanoparticles: An effective antifungal agent against *Aspergillus niger* and *Fusarium oxysporum*. *Appl. Microbiol. Biotechnol.* **90**, 733–743.

Choudhury, S. R., Roy, S., Goswami, A., and Basu, S. (2012). Polyethylene glycol-stabilized sulphur nanoparticles: An effective antimicrobial agent against multidrug-resistant bacteria. *J. Antimicrob. Chemother.* **67**, 1134–1137.

Clift, M. J. D., Rothen-Rutishauser, B., Brown, D. M., Duffin, R., Donaldson, K., Proudfoot, L., Guy, K., and Stone, V. (2008). The impact of different nanoparticle surface chemistry and size on uptake and toxicity in a murine macrophage cell line. *Toxicol. Appl. Pharmacol.* **232**, 418–427.

Coulter, J. B., O'Driscoll, C. M., and Bressler, J. P. (2013). Hydroquinone increases 5-hydroxymethylcytosine formation through ten eleven translocation 1 (TET1) 5-methylcytosine dioxygenase. *J. Biol. Chem.* **288**, 28792–28800.

Cui, Y., Choudhury, S. R., and Irudayaraj, J. (2016). Epigenetic toxicity of trichloroethylene: A single-molecule perspective. *Toxicol. Res.* **5**, 641–650.

Delatte, B., Jeschke, J., Defrance, M., Bachman, M., Creppe, C., Calonne, E., Bizet, M., Deplus, R., Marroquí, L., Libin, M., *et al.* (2015). Genome-wide hydroxymethylcytosine pattern changes in response to oxidative stress. *Sci. Rep.* **5(12714)**, 1–10.

Ehmann, F., Sakai-Kato, K., Duncan, R., Hernan Perez de la Ossa, D., Pita, R., Vidal, J. M., Kohli, A., Tothfalusi, L., Sanh, A., Tinton, S., *et al.* (2013). Next-generation nanomedicines and nanosimilars: EU regulators' initiatives relating to the development and evaluation of nanomedicines. *Nanomedicine (Lond.)* **8**, 849–856.

Ehrlich, M. (2009). DNA hypomethylation in cancer cells. *Epigenomics* **1**, 239–259.

Fan, Z., and Lu, J. G. (2005). Zinc oxide nanostructures: Synthesis and properties. *J. Nanosci. Nanotechnol.* **5**, 1561–1573.

Gauss, K. A., Bunger, P. L., Larson, T. C., Young, C. J., Nelson-Overton, L. K., Siemsen, D. W., and Quinn, M. T. (2005). Identification of a novel tumor necrosis factor alpha-responsive region in the NCF2 promoter. *J. Leukoc. Biol.* **77**, 267–278.

Gerber, C., and Lang, H. P. (2006). How the doors to the nanoworld were opened. *Nat. Nanotechnol.* **1**, 3–5.

Gornicka, A., Morris-Stiff, G., Thapaliya, S., Papouchado, B. G., Berk, M., and Feldstein, A. E. (2011). Transcriptional profile of genes involved in oxidative stress and antioxidant defense in a dietary murine model of steatohepatitis. *Antioxid. Redox Signal* **15**, 437–445.

Guo, J. U., Su, Y., Zhong, C., Ming, G. L., and Song, H. (2011). Hydroxylation of 5-methylcytosine by TET1 promotes active DNA demethylation in the adult brain. *Cell* **145**, 423–434.

Heim, J., Felder, E., Tahir, M. N., Kaltbeitzel, A., Heinrich, U. R., Brochhausen, C., Mailander, V., Tremel, W., and Brieger, J. (2015). Genotoxic effects of zinc oxide nanoparticles. *Nanoscale* **7**, 8931–8938.

Hondow, A. P B a R M D B a N S. (2014). Measuring in vitro cellular uptake of nanoparticles by transmission electron microscopy. *J. Phys.: Conf. Ser.* **522**, 012058.

Huang, C. C., Aronstam, R. S., Chen, D. R., and Huang, Y. W. (2010). Oxidative stress, calcium homeostasis, and altered gene expression in human lung epithelial cells exposed to ZnO nanoparticles. *Toxicol. in Vitro* **24**, 45–55.

Huang, Y., Chavez, L., Chang, X., Wang, X., Pastor, W. A., Kang, J., Zepeda-Martinez, J. A., Pape, U. J., Jacobsen, S. E., Peters, B., *et al.* (2014). Distinct roles of the methylcytosine oxidases Tet1 and Tet2 in mouse embryonic stem cells. *Proc. Natl. Acad. Sci. U.S.A.* **111**, 1361–1366.

Jaenisch, R., and Bird, A. (2003). Epigenetic regulation of gene expression: How the genome integrates intrinsic and environmental signals. *Nat. Genet.* **33(Suppl)**, 245–254.

Jirtle, R. L., and Skinner, M. K. (2007). Environmental epigenomics and disease susceptibility. *Nat. Rev. Genet.* **8**, 253–262.

Jones, N., Ray, B., Ranjit, K. T., and Manna, A. C. (2008). Antibacterial activity of ZnO nanoparticle suspensions on a broad spectrum of microorganisms. *FEMS Microbiol. Lett.* **279**, 71–76.

Kao, Y. Y., Chen, Y. C., Cheng, T. J., Chiung, Y. M., and Liu, P. S. (2012). Zinc oxide nanoparticles interfere with zinc ion homeostasis to cause cytotoxicity. *Toxicol. Sci.* **125**, 462–472.

Kato, T., Morita, M. T., and Tasaka, M. (2010). Defects in dynamics and functions of actin filament in *Arabidopsis* caused by the dominant-negative actin fiz1-induced fragmentation of actin filament. *Plant Cell Physiol.* **51**, 333–338.

Li, N., Xia, T., and Nel, A. E. (2008). The role of oxidative stress in ambient particulate matter-induced lung diseases and its implications in the toxicity of engineered nanoparticles. *Free Radic. Biol. Med.* **44**, 1689–1699.

Lim, S. O., Gu, J. M., Kim, M. S., Kim, H. S., Park, Y. N., Park, C. K., Cho, J. W., Park, Y. M., and Jung, G. (2008). Epigenetic changes induced by reactive oxygen species in hepatocellular carcinoma: Methylation of the E-cadherin promoter. *Gastroenterology* **135**, 2128–2140, 2140.e1–8.

Lin, D., and Xing, B. (2007). Phytotoxicity of nanoparticles: Inhibition of seed germination and root growth. *Environ. Pollut.* **150**, 243–250.

Nel, A., Xia, T., Madler, L., and Li, N. (2006). Toxic potential of materials at the nanolevel. *Science* **311**, 622–627.

Neumeier, M., Weigert, J., Schäffler, A., Weiss, T. S., Schmidl, C., Büttner, R., Bollheimer, C., Aslanidis, C., Schölmerich, J., and Buechler, C. (2006). Aldehyde oxidase 1 is highly abundant in hepatic steatosis and is downregulated by adiponectin and fenofibric acid in hepatocytes in vitro. *Biochem. Biophys. Res. Commun.* **350**, 731–735.

Oberdorster, G., Sharp, Z., Atudorei, V., Elder, A., Gelein, R., Kreyling, W., and Cox, C. (2004). Translocation of inhaled ultrafine particles to the brain. *Inhal. Toxicol.* **16**, 437–445.

Perreault, F., Pedroso Melegari, S., Henning da Costa, C., de Oliveira Franco Rossetto, A. L., Popovic, R., and Gerson Matias, W. (2012). Genotoxic effects of copper oxide nanoparticles in Neuro 2A cell cultures. *Sci. Total Environ.* **441**, 117–124.

Pronk, T. E., van der Veen, J. W., Vandebriel, R. J., van Loveren, H., de Vink, E. P., and Pennings, J. L. (2014). Comparison of the molecular topologies of stress-activated transcription factors HSF1, AP-1, NRF2, and NF-kappaB in their induction kinetics of HMOX1. *Biosystems* **124**, 75–85.

Pujalté, I., Passagne, I., Brouillaud, B., Tréguer, M., Durand, E., Ohayon-Courtès, C., and L'Azou, B. (2011). Cytotoxicity and oxidative stress induced by different metallic nanoparticles on human kidney cells. *Part. Fibre Toxicol.* **8**, 1–16.

Quan, X., Lim, S. O., and Jung, G. (2011). Reactive oxygen species downregulate catalase expression via methylation of a CpG island in the Oct-1 promoter. *FEBS Lett.* **585**, 3436–3441.

Ramadass, R., and Bereiter-Hahn, J. (2008). How DASPMI reveals mitochondrial membrane potential: Fluorescence decay kinetics and steady-state anisotropy in living cells. *Biophys. J.* **95**, 4068–4076.

Rana, S., and Kalaichelvan, P. T. (2013). Ecotoxicity of nanoparticles. *ISRN Toxicol.* **2013**, 574648.

Ricci, J. E., Gottlieb, R. A., and Green, D. R. (2003). Caspase-mediated loss of mitochondrial function and generation of reactive oxygen species during apoptosis. *J. Cell Biol.* **160**, 65–75.

Rihn, B. H., Bottin, M. C., Coulais, C., Rouget, R., Monhoven, N., Baranowski, W., Edorh, A., and Keith, G. (2000). Genotoxicity of 3-methylcholanthrene in liver of transgenic big Blue mice. *Environ. Mol. Mutagen* **36**, 266–273.

Robertson, K. D., Uzvolgyi, E., Liang, G., Talmadge, C., Sumegi, J., Gonzales, F. A., and Jones, P. A. (1999). The human DNA methyltransferases (DNMTs) 1, 3a and 3b: Coordinate mRNA expression in normal tissues and overexpression in tumors. *Nucleic Acids Res.* **27**, 2291–2298.

Sarkar, S., Sharma, C., Yog, R., Periakaruppan, A., Jejelowo, O., Thomas, R., Barrera, E. V., Rice-Ficht, A. C., Wilson, B. L., and Ramesh, G. T. (2007). Analysis of stress responsive genes induced by single-walled carbon nanotubes in BJ Foreskin cells. *J. Nanosci. Nanotechnol.* **7**, 584–592.

Sharma, V., Anderson, D., and Dhawan, A. (2012). Zinc oxide nanoparticles induce oxidative DNA damage and ROS-triggered mitochondria mediated apoptosis in human liver cells (HepG2). *Apoptosis* **17**, 852–870.

Sharma, V., Shukla, R. K., Saxena, N., Parmar, D., Das, M., and Dhawan, A. (2009). DNA damaging potential of zinc oxide nanoparticles in human epidermal cells. *Toxicol. Lett.* **185**, 211–218.

Shen, C., James, S. A., de Jonge, M. D., Turney, T. W., Wright, P. F., and Feltis, B. N. (2013). Relating cytotoxicity, zinc ions, and reactive oxygen in ZnO nanoparticle-exposed human immune cells. *Toxicol. Sci.* **136**, 120–130.

Singh, P., and Nanda, A. (2014). Enhanced sun protection of nano-sized metal oxide particles over conventional metal oxide particles: An in vitro comparative study. *Int. J. Cosmet. Sci.* **36**, 273–283.

Stricker, J., Falzone, T., and Gardel, M. L. (2010). Mechanics of the F-actin cytoskeleton. *J. Biomech.* **43**, 9–14.

Tahiliani, M., Koh, K. P., Shen, Y., Pastor, W. A., Bandukwala, H., Brudno, Y., Agarwal, S., Iyer, L. M., Liu, D. R., Aravind, L., *et al.* (2009). Conversion of 5-methylcytosine to 5-hydroxymethylcytosine in mammalian DNA by MLL partner TET1. *Science* **324**, 930–935.

Teeguarden, J. G., Hinderliter, P. M., Orr, G., Thrall, B. D., and Pounds, J. G. (2007). Particokinetics in vitro: Dosimetry considerations for in vitro nanoparticle toxicity assessments. *Toxicol. Sci.* **95**, 300–312.

Turpaev, K. T. (2002). Reactive oxygen species and regulation of gene expression. *Biochemistry (Mosc)* **67**, 281–292.

Turrens, J. F. (2003). Mitochondrial formation of reactive oxygen species. *J Physiol.* **552**, 335–344.

Wang, B., Feng, W. Y., Wang, T. C., Jia, G., Wang, M., Shi, J. W., Zhang, F., Zhao, Y. L., and Chai, Z. F. (2006). Acute toxicity of nano- and micro-scale zinc powder in healthy adult mice. *Toxicol. Lett.* **161**, 115–123.

Wang, F., Gao, F., Lan, M., Yuan, H., Huang, Y., and Liu, J. (2009). Oxidative stress contributes to silica nanoparticle-induced cytotoxicity in human embryonic kidney cells. *Toxicol. in Vitro* **23**, 808–815.

Wang, J., Deng, X., Zhang, F., Chen, D., and Ding, W. (2014). ZnO nanoparticle-induced oxidative stress triggers apoptosis by activating JNK signaling pathway in cultured primary astrocytes. *Nanoscale Res. Lett.* **9**, 117

Wenk, J., Brenneisen, P., Wlaschek, M., Poswig, A., Briviba, K., Oberley, T. D., and Scharffetter-Kochanek, K. (1999). Stable overexpression of manganese superoxide dismutase in mitochondria identifies hydrogen peroxide as a major oxidant in the AP-1-mediated induction of matrix-degrading metalloprotease-1. *J. Biol. Chem.* **274**, 25869–25876.

Westmoreland, C., Benford, D. J., Eales, L. J., and Grasso, P. (1994). Investigations into the mechanisms of carcinogen-induced nuclear enlargement in HeLa S3 cells in vitro. *Toxicol. in Vitro* **8**, 1139–1150.

Wilhelmi, V., Fischer, U., Weighardt, H., Schulze-Osthoff, K., Nickel, C., Stahlmecke, B., Kuhlbusch, T. A., Scherbart, A. M., Esser, C., Schins, R. P., *et al.* (2013). Zinc oxide nanoparticles induce necrosis and apoptosis in macrophages in a p47phox- and Nrf2-independent manner. *PLoS One* **8**, e65704.

Wu, C., Qiao, X., Chen, J., Wang, H., Tan, F., and Li, S. (2006). A novel chemical route to prepare ZnO nanoparticles. *Mater. Lett.* **60**, 1828–1832.

Wu, H., and Zhang, Y. (2011). Mechanisms and functions of Tet protein-mediated 5-methylcytosine oxidation. *Genes Dev.* **25**, 2436–2452.

Wu, Q., and Ni, X. (2015). ROS-mediated DNA methylation pattern alterations in carcinogenesis. *Curr. Drug Targets* **16**, 13–19.

Xia, T., Kovochich, M., Liong, M., Madler, L., Gilbert, B., Shi, H., Yeh, J. I., Zink, J. I., and Nel, A. E. (2008). Comparison of the mechanism of toxicity of zinc oxide and cerium oxide nanoparticles based on dissolution and oxidative stress properties. *ACS Nano* **2**, 2121–2134.

Yokel, R. A., and MacPhail, R. C. (2011). Engineered nanomaterials: Exposures, hazards, and risk prevention. *J. Occup. Med. Toxicol. (Lond. Engl.)* **6**, 7.

Yu, K. N., Yoon, T. J., Minai-Tehrani, A., Kim, J. E., Park, S. J., Jeong, M. S., Ha, S. W., Lee, J. K., Kim, J. S., and Cho, M. H. (2013). Zinc oxide nanoparticle induced autophagic cell death and mitochondrial damage via reactive oxygen species generation. *Toxicol. in Vitro* **27**, 1187–1195.

Zhao, B., Yang, Y., Wang, X., Chong, Z., Yin, R., Song, S. H., Zhao, C., Li, C., Huang, H., Sun, B. F., *et al.* (2014). Redox-active quinones induces genome-wide DNA methylation changes by an iron-mediated and Tet-dependent mechanism. *Nucleic Acids Res.* **42**, 1593–1605.

Zhao, J., Xu, L., Zhang, T., Ren, G., and Yang, Z. (2009). Influences of nanoparticle zinc oxide on acutely isolated rat hippocampal CA3 pyramidal neurons. *Neurotoxicology* **30**, 220–230.

Ziech, D., Franco, R., Pappa, A., and Panayiotidis, M. I. (2011). Reactive oxygen species (ROS)-induced genetic and epigenetic alterations in human carcinogenesis. *Mutat. Res.***711**, 167–173.